Improving Navigation Precision of Milling Operations in Surgical Robotics

Philipp J. Stolka and Dominik Henrich
Lehrstuhl für Angewandte Informatik III
(Robotik und Eingebettete Systeme)
Universität Bayreuth, D-95447 Bayreuth, Germany
{philipp.stolka, dominik.henrich}@uni-bayreuth.de

***Abstract* – Current approaches to establish or improve precision of registration and execution in (surgical) robotics, especially milling applications, mostly aim at determining an exact relationship between intervention area and the robot. However, this is subject to quality deterioration due to positional shifts and deformations under load. Therefore, in this work we describe two approaches to define and measure the actual tool position more accurately – by optical and force measurements – to both ease static and dynamic registration and estimate tool and other deformations.**

***Keywords*: precision, surgical robotics, milling, navigation, registration, optical tracking, force sensing, deformation estimation**

I. Introduction

Robots are widely used in surgical settings. They assist in passive tasks like camera holding as well as in more active situations like servoing of fixtures, endoscopic guidance, and actual tissue interaction [13], [17]. The latter includes both open interventions with direct access to the operation site (*situs*), and deeper-lying, occluded operations through small incisions. While the first real applications of surgical robotic systems have been soft tissue interventions, orthopedic operations have been long common as well. Contrary to conventional machining, the subject of interest in surgical applications is a human patient, whose anatomy is highly individual and thus necessitates careful planning based on pre-operative data.

Detrimental influences to precision include inaccuracies during all of the process phases – sensing, planning, registration, positioning, motion, and tool errors. When using an industrial-grade, approved-for-medical-use robot, and when planning on data acquired from sources like the gold standard of medical imaging, i.e. computer tomography (CT), the two largest remaining single sources of error are the precision of the pre- and intraoperative static and dynamic registration and inaccuracies caused by the used tool itself.

The well-known problem of *registration* deals with establishing a known spatial relationship between data and patient, so that intra-operative localization of tools etc. corresponds to their actual position [11]. This requires a precise method for determining the position of the patient, the tools, and the robot, if applicable. However, the tools and the robot can be subject to external forces and moments as well, distorting its supposedly fixed geometry and deteriorating the quality of the intervention result, since the position of the tool is only known with insufficient precision then. Especially when using intraoperative data from local sensors for map-building and navigation, exact location data is highly important [15]. Therefore, in this work we describe two approaches to improve the precision of the measured tool position in order to make the outcome of high-precision operations like milling more predictable.

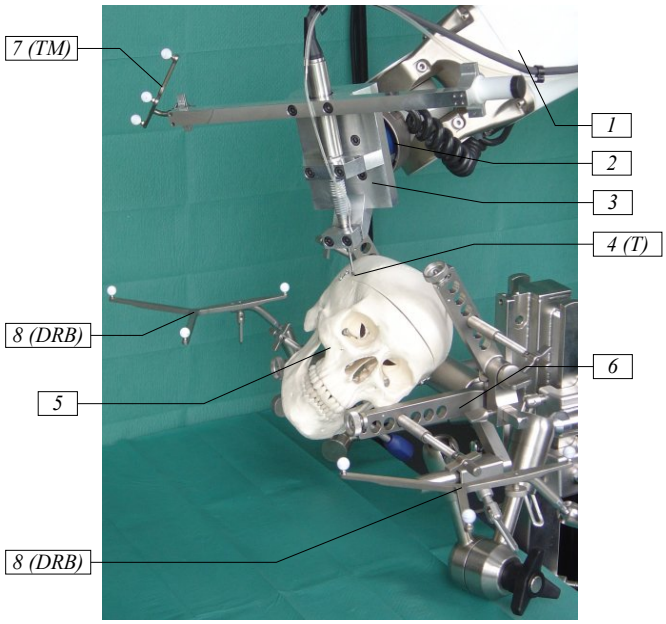

Figure 1: Setup of the RONAF system – robot arm (1) with F/T sensor (2), tool holder (3), surgical miller tip (4), a skull phantom (5), fixatures (6), and infrared-reflective markers of the tool (7) and the robot base (8)

First, we give an overview of the state of the art in Section II with references to related work. In Section III, the navigation cycles and registration methods of the presented robot system RONAF (Figure 1) are described, while Section IV presents the system architecture and components. A more precise problem description and the proposed additional features are found in Section V. Section VI highlights the achievable results of the combined approaches. Finally, Section VII concludes with an outlook on further research and developments related to this work.

II. State of the art

In robot-assisted surgical systems, registration is often related to determining the spatial relationship between pre-operative planning data and the intra-operatively acquired reference set. However, this registration often cannot be assumed to be fixed, or static. It is difficult to completely immobilize the patient, and nearly impossible to do so when dealing with soft tissue. Motion of the patient (*patient shift*) and motion of soft tissue like skin, the brain, or other inner organs (*tissue shift)* are inevitable results. It is sometimes possible, although undesirable due to implantation trauma, to attach bone-fixed markers (*fiducials*) in the intervention area to make them clearly visible in imaging data as well as physically approachable with the robot, as early commercial systems like Robodoc or CASPAR demonstrated [16] for *static* (initial) registration. With appropriate markers, it is possible to establish *dynamic* (persistent) registration with optical or electromagnetical tracking devices as well. However, often this is not an option, especially for endoscopic surgery. Therefore, non-invasive tracking methods are generally preferred nowadays, like surface-mounted optical markers for tracking skin motion, clamped markers for head motion (e.g. the VBH head holder), or servoing based on visual clues from video streams [2]. All of these result in dynamic registration relationships and aim at reducing the errors between expected and actual position of the intervention area. Alternatives for static registration include point-like anatomical landmarks, defined with pointing devices, or shape-based methods of registering geometrical features from image data, like surfaces, crests, or sets of points. Those methods, possibly combined with atlas databases of deformable organ models, may even make preoperative imaging unnecessary (e.g. in the BrainLab VectorVision knee TKR). In general, optical tracking seems to offer the best compromise of precision and speed available for both static and dynamic registration.

Deformation of the robot has been discussed for only a few surgical robotic systems, including e.g. the sensor-aided serial robot system in [5], where deformations of up to 1.5mm are reported for milling operations. However, this may be interesting for high-precision autonomous robots like e.g. the CRIGOS hexapod orthopaedic system, for long, teleoperated arms like the ZEUS endoscopic system, and has already been discussed for industrial systems, e.g. the nuclear inspection 4 degrees-of-freedom manipulator Cobra, where extensive modelling based on deflection matrices for individual links is performed, and accuracy could be improved from 1.5in to 0.09in under 30lbs load [12]. In another medical deformation modelling work [3], a patient positioner's accuracy was improved from 5...8mm to 0.4mm through representation of geometric and elastic errors for six axes and calibration with a laser tracking device. Freehand robot-less navigation with force-based deflection compensation is discussed e.g. in [1]. In the bone milling applications of the presented RONAF system [9], tool forces of up to 30N suggest deformation modelling.

Deformations of tissues and other surgical enviroments are usually represented by finite element models and mainly used for training and simulation. They are of little interest here because of their generally lower requirements for exact representation of actual behaviour.

It can be concluded that for a description of the achievable overall accuracy of milling operations, more information about first the precision of registration based on optically tracked pointers, and second about milling deformation effects, is necessary to determine precision of such robot-assisted surgical milling processes.

III. Navigation Principles

Current surgical robot systems mainly rely on two sources of navigation information: global data sampled during a planning phase before process execution (*preparation phase*), which is then used statically in a spatial context for global navigation, and local data sampled during the process (*execution phase*), which is fed back and used in a non-spatial context in open- or closed-loop process control. The former may have insufficient spatial resolution, be difficult to segment, or expensive, while the latter only persists during the instant of sampling and is discarded immediately after entering into the control cycles. However, especially with autonomous robots, additional information – intraoperative, spatial, current, and persistent sensor data – proves necessary to cope with uncertainty, measurement errors, and incompleteness of data.

The following Subsections A through D describe four navigation principles in medical robotics (Figure 2). This paper is focused mainly on cycles B and C.

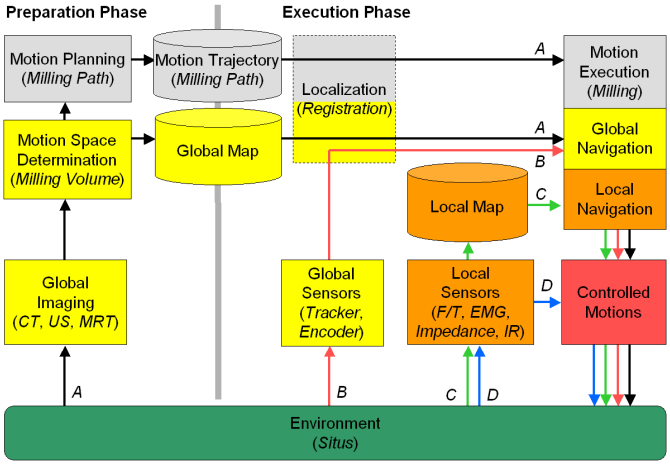

Figure 2: General navigation system architecture including the four navigation principles (A through D), with examples from surgery [10]

A. Global Navigation, Preoperative Data

Global navigation with a preoperative map requires preoperative imaging of the intervention region and is used mainly for planning. Locations and paths can be described within this map in a global fashion. This map needs to be registered with the environment before process execution. No strict temporal restrictions between data sampling and process execution are imposed. Global, preoperative sensors include computed tomography (*CT*), ultrasound (*US*), and magnetic resonance tomography (*MRT*).

B. Global Navigation, Intraoperative Data

Global navigation based on an intraoperatively acquired map is conceptually similar to the previous principle. One has knowledge of the complete environment via a global map. However, acquisition may take place occasionally during the intervention, thus updating the environment representation. External trackers (optical, electromagnetic, and others) and robot or localizer encoders provide suitable data.

C. Local Navigation

In local navigation, execution begins without prior knowledge, and an initially empty local map is continuously filled with information sampled during execution. This new information has two important properties: it is local, and it may provide more current and precise knowledge of the environment than global sensors could. However, for correct mapping it is extremely important to have precise and current location information. Local sensors can be force/torque sensors (*F/T*), electromyography (*EMG*), electrical impedance, or infrared (*IR*) sensors.

D. Control

Control encompasses the sampling of data elements from the process – using the same intraoperative sensors as cycles B and C –, computing a reaction that is fed to an actuating element, and possibly providing a feedback path to the controller for closed-loop control. Control does not require spatial information; it serves as a reactive navigation principle without persistent map-building functionality.

IV. Application

The scope of application is the automated milling of cavities in skull bone for subdermal implantation of hearing aids, performed by the medical robotic system RONAF ("Robot-based navigation for milling at the lateral skull base") [9]. One step of the process is the removal of bone material from the thin calotte in the shape of flat amplifier components (Figure 3), with the possible complication of breakthrough into the skull interior and rupture of the sensitive meningeal (*dura mater*) enclosing the brain.

The robot is an industrial model (Stäubli RX90) retrofitted for medical use in hip and knee endoprosthesis milling applications (CASPAR, by Orto-Maquet) regarding speed and safety. Sensors include a 6D force/torque (*F/T*) sensor (JR3 90M31A using strain gage bridges, max. sensing range 63N/5Nm, resolution 1:4000), a room microphone, ultrasound, and an NDI Polaris infrared-optical tracking system (*OTS*; measured repeatability accuracy 0.05mm RMS after warm-up phase, specified absolute accuracy 0.35mm RMS, work volume silo-shaped ~(1000mm)³, data rate 20...60Hz). The tool is a surgical mill (electrically driven miller Aesculap microtron EC/GD622, up to 30.000 rpm) mounted perpendicularly to the robot tool flange to minimize deformation (Figure 1).

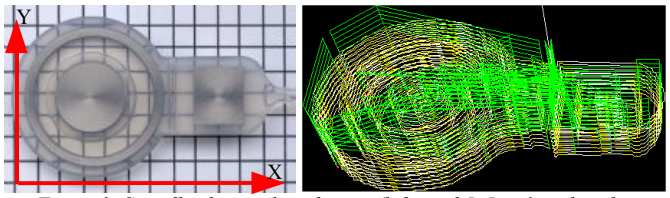

Figure 3: Soundbridge implant dummy (left; grid 5x5mm², with right-handed coordinate system), generated layered concentrical milling path (right)

V. Registration and Position Correction

In this section, the possible causes of imprecise operation of surgical robots are discussed, with the most influential ones pointed out. Then, two features of the RONAF system will be described which serve to improve the result.

Errors influencing the precision of the final intervention result originate in many phases of the process:

- *Sensing error* can be both mislocated features (i.e. correct samples at wrong locations) and misrecognized features (i.e. measuring a wrong environment feature at a certain location). The latter is mostly a segmentation or classification error, which is outside of the scope of methods to improve precision, while the former might be representable.
- *Planning error* is caused by misestimation or ignorance of system parameters, like robot dynamics, tool sizes, tool effectivity etc. Careful definition of those parameters helps to eliminate these effects. Logical errors arising from the omission of constraints are included, as well as special examples like non-optimal placement of the intervention volume relative to the patient [19], but this is beyond the scope of this consideration as well.
- *Registration error* is the difference between the expected location of world model features as defined through some registration procedure expressed in system, e.g. robot coordinates, and their actual counterparts' location in the environment. This error is introduced by imprecise localization of environment features or by faulty matching of features between sensed model and real environment. Registration errors can be both static – caused by imprecise initial matching – and dynamic – caused by gradual or sudden drift of the environment from its expected position.
- *Position error* in the context of the present work is the difference between expected position $\boldsymbol{p}_{exp}$ – of the tool, robot, or other entities – in robot work space as measured or commanded, and the actual position $\boldsymbol{p}_{act}$ as resulting from the combination of servoing errors, encoder inaccuracies, miscalibrations and misregistration, and deformation from external loads.
- *Motion error* has a dynamic origin, i.e. inaccuracies in following the planned path caused by operating the robot beyond its maximal speed or acceleration, or originates in planning, i.e. caused by faulty or at least unexpected behaviour of the motion planner at system level, both of which can be ruled out by conservative path planning and extensive testing.
- *Tool error*, finally, is inaccuracy of execution due to insufficient modelling of any actual tool operation, and can include effects like the width of saw cuts, tearing due to milling, and other operation-related issues.

In this work, we describe two methods to reduce the overall error. Working on top of and additionally to the primary localization method of reading joint position encoders of the

robot, use of optical tracking and deformation estimation helps to reduce registration and sensing/position errors.

Optical tracking provides a source of position information independent from the internal robot encoders, and can serve to reduce static and dynamic registration error (Subsection A). Deformation of the robot and tool combination can be estimated to reduce the position error (Subsection B). This also helps with sensing error as far as local sensors are concerned. Planning error, motion error, and tool error are not considered here, because they have already been dealt with for the presented task (like optimal planning [19]), are irrelevant (only slow motions) or their causes cannot be changed (like the type of used tool), respectively.

A. Optical registration

One very simple way of inducing a static and rigid registration relationship between the planned path and its execution site is the definition of a local coordinate system (*frame*) by providing three or more distinct points. This can be achieved e.g. by a force-following procedure (guiding the robot manually by imposing forces on the tool [14]). However, this is undesirable for several reasons – it requires quite intimate knowledge of the system behaviour, the surgeon needs to interact physically with the robot, and it is not feasible to define many points due to time requirements (15...25sec/point on average in our earlier experiments; accuracy 0.5...1mm). On the other hand, registration of image data and the execution site using fiducials, which is another common method for establishing registration with image data, is undesirable and necessitates an imaging step. Therefore, we aim at both defining and registering features with hand-held pointers (Figure 4), similar to imaging-free procedures for orthopedic interventions, by tracking with an infrared optical tracking system (OTS). Further registration of other image modalities with the patient can then be performed with intraoperative imaging procedures like ultrasound thickness measurements [7], which additionally serve to improve the quality of planning data.

These pointers can be used to define single points in space, delineate regions on surfaces, or define trajectories. The markers attached to the pointers carry local frames and can be basically arbitrarily attached to the pointer itself. Therefore, before any points can be provided that way, the pointer needs to be calibrated to determine the transformation ${}^{A}\boldsymbol{p}_{Z}$ from the marker A to the pointer tip Z or, in other words, the position of the tip in the marker frame. A technical drawing to do so may not be available, so a more general method would be preferable.

Our approach is based on pivoting (rotating) the pointer around a fixed end point. The optical tracking system continuously reports the locations ${}^{\mathrm{OTS}}\boldsymbol{p}_{\mathrm{A,i}}$ of the local marker frame in OTS coordinates, which are collected and continuously

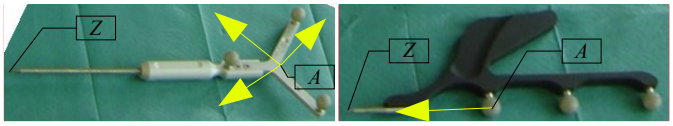

Figure 4: Two pointers (6D and 5D) with respective (example) local frames (origin A) and tips (Z)

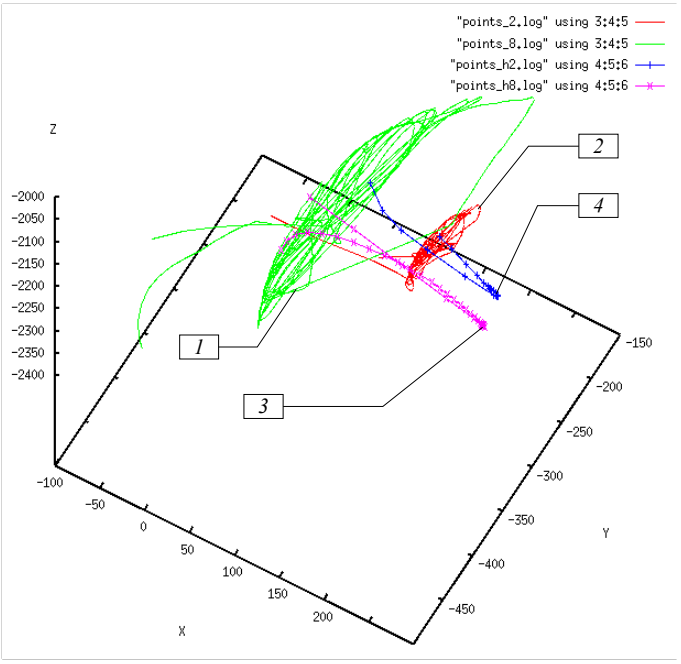

Figure 5: Traces of two optical pointers (1, 2) with resulting fitted sphere centres (3, 4) in OTS coordinates

subjected to a sphere fitting algorithm to determine whether they lie on a sphere surface, and extract its parameters. While some sphere can always be fitted to the location samples in the current window, it is only during pivoting that the successive sphere centres ${}^{\mathrm{OTS}}\boldsymbol{c}_{\mathrm{A,i}}$ and radii $\boldsymbol{r}_{\mathrm{A,i}}$ stabilize long enough on valid values. When those parameters are established, the calibration is finalized by taking one more location sample ${}^{\mathrm{OTS}}\boldsymbol{p}_{\mathrm{A}}$ and applying its inverse on the determined centre ${}^{\mathrm{OTS}}\boldsymbol{c}_{\mathrm{A}} = {}^{\mathrm{OTS}}\boldsymbol{p}_{\mathrm{Z}}$:

$$ {}^{A}\boldsymbol{p}_{Z} = {}^{A}\boldsymbol{M}_{OTS} \cdot {}^{OTS}\boldsymbol{p}_{Z} \quad \text{, where} \quad {}^{A}\boldsymbol{M}_{OTS} = ({}^{OTS}\boldsymbol{p}_{A})^{-1} $$

The whole semi-automatic pointer calibration procedure requires the user to pivot the pointer for a short time to define a stable end point, switches into fitting mode to determine it exactly, and switches back after one second (Figure 5).

The sphere fitting is done by a Modified Least Squares method (MLS), yielding a sphere centre which minimizes the sum of the squared distances from this centre to all planes which are bisectors of pairs of sampled points [18]. The radius can then be computed as the mean of the resulting distances between samples and the centre. This method is comparatively robust against both outliers and close neighbors. Furthermore, it can be expressed in closed form and is thus a reliable real-time algorithm.

The same procedure is used to determine the transformation ${}^{\mathrm{TM}}\boldsymbol{M}_{\mathrm{T}}$ from tool marker *TM* to tool tip *T* to calibrate the tool (cf. Figure 1). This is important since the tool marker must allow quick reconfiguration for good visibility in the operating room. However, contrary to pointer calibration, for full registration between the tool (and thus the robot) and the OTS, their relative orientation needs to be determined, too. This is achieved with two additional small motions along the tool frame X and Y axes, which together immediately span up the respective coordinate system ${}^{\mathrm{OTS}}\boldsymbol{M}_{\mathrm{T}}$ when projected into OTS coordinates. However, the absolute positioning accuracy of the robot may mar the calibration quality.

Thus, the transformation relations between the OTS and the tool marker *TM*, the tool marker and the tool tip *T*, and thus the tool tip and any hand-held pointer tips $\boldsymbol{Z}_j$ are known. Additional markers at the robot base serve as dynamic reference bases DRB_k to detect accidental motion of the OTS.

B. Deformation Estimation

An important source of position errors is motion under contact, i.e. the influence of mechanical load to the whole structure (base, robot, tool holder, and tool) on the position of the tool tip. This influence results in wrong position information, i.e. incorrectly estimated tool tip position, due to elastic deformation (bending or deflection). To model and estimate this error, it is necessary to characterize the possible loads and their mechanical effects to the system structure first. Several simplifying assumptions can be made prior to modelling.

First, the application allows mechanical contacts between robot and environment only at the tool tip, other significant loads to the arm or base are prohibited. Therefore it is sufficient to investigate the effects of forces and torques at the tool tip. Second. as the relative size of the tool tip – i.e. the miller head – is negligibly small (~2...5mm) compared to its distance from the F/T sensor (~130mm), it can be approximated as a dimensionless point of force application on an appropriate beam lever. As a practical consequence, torques on the tool tip apart from the one along the tool axis cannot be applied. Similarly, tensile, compressive, or shearing forces need not be considered. Third, the miller's electric motor is not powerful enough to effect relevant torsion of the remaining structure from the fixed position of the miller tip.

In a first step, the stiffness of the whole structure needs to be estimated. During the later online phase, tip displacements are accounted for by adding a corresponding error vector. Since there is no structural reason – like predetermined bending directions – for non-isometric deformation, the error model can be assumed as basically a linear combination of orthogonal deformations. Stiffness data gathered from the experiments (see Subsection VI.B.I) exhibited highly linear force-to-deflection ratios $\boldsymbol{k}_i$, $i = x, y, z$, so the deformations can be modelled as linear relationships. Together, the 3D deformation $\Delta\boldsymbol{p}$ caused by the force vector $\boldsymbol{F}$ is representable by the diagonal stiffness matrix as

$$\Delta\boldsymbol{p}(\boldsymbol{F})\cdot\begin{pmatrix} k_x & 0 & 0 \\ 0 & k_y & 0 \\ 0 & 0 & k_z \end{pmatrix} = \boldsymbol{F}$$

The position measurements $\boldsymbol{p}_{meas}$ are corrected with this deformation to the estimate

$$\boldsymbol{p}_{corr} = \boldsymbol{p}_{meas} + \Delta\boldsymbol{p}(\boldsymbol{F})$$

This force-based deformation measurement allows more precise mapping when used in the local navigation cycle, since sensor samples can then be entered into the map at their actual location of origin [15]. Currently this does not include correction of the tip position itself yet.

VI. Experiments and Results

Experiments were conducted to determine the attainable precision of the optical tracking method (Subsection A) and the deformation estimation (Subsection B).

A. Optical Tracking

Determining the precision of the OTS subsystem includes measuring the precision of the pointer calibration (Subsection A.I), as the pointers will be used later to define points in the robot frame, and the registration of robot and OTS for correct projection of optically sampled points into the robot frame (Subsection A.II).

A.I Pointer Calibration

First, the precision of the sphere fitting procedure was determined experimentally. Data samples were generated by pivoting one pointer continuously around its tip *Z* and taking the coordinates of its (rotating) marker *A* as returned by the OTS. The standard deviation (also root-mean-squared error/*RMS*) of n=50 repeatedly collected sphere centres was computed as $s_C = 0.33$mm (mean) for a pivoting radius of 210mm and $s_C = 0.25$mm (mean) for a pivoting radius of 88mm. The maximum distance between sphere centres was about 2.6mm, with the majority less than 1.2mm apart. These values can be interpreted as the maximum accuracy achievable for OTS-based definition of 3D points, as they describe the precision of the sphere fitting based calibration.

The accuracy of the OTS-based pointing itself was tested then. The tip *Z* of a tool with radius 210mm was pointed at constant locations with different angles, and the distance between successive tip position samples computed. Being highly dependent on the quality of the initial calibration and the type of pointer used, this distance oscillated around mean $\mu(d_Z) = 0.69$mm (0.42mm excluding outliers) with sample standard deviation $s_Z = 0.32$mm.

Finally, the "two-sided" precision of the calibration procedure was tested with two pointers. After calibrating each (i.e. determining the ${}^{Ai}\boldsymbol{p}_{Zi}$), their tips $Z_{1,2}$ were pointed at each other at different locations and angles within the OTS work volume. The resulting distance between both tips can be interpreted as the maximum achievable precision at which any two OTS-tracked objects can be controlled relative to each other, and was determined to be around $\mu(d_{ZZ}) = 0.5$mm.

A.II Robot-Camera Registration

The tip-to-marker registration ${}^{TM}\boldsymbol{M}_T$ of the tool was tested with a hand-held pointer in a similar setup as the two-sided precision above. The pointer tip *Z* was pointed at the tool tip *T*, both of which have been calibrated as described above. Then, the distance between the (single) computed locations of *T* and *Z* at different angles of pointer and tool was calculated; it amounts to mean $\mu(d_{TZ}) = 2.5$mm.

Finally, the tool-to-OTS registration ${}^{OTS}\boldsymbol{M}_T$ was tested. The robot encoders were assumed to be "ground truth", i.e. giving accurate positions relative to the robot base, and were used to define a set of positions ${}^{ROB}\boldsymbol{p}_i$ within the relevant robot workspace by force following. The positions ${}^{OTS}\boldsymbol{p}_i \approx {}^{ROB}\boldsymbol{p}_i$

were demonstrated a second time with a pivoting pointer relative to the origin of the tool calibration position. The mean distance between corresponding pairs of positions was then measured as $\mu(d_{TP}) = 2...4$mm. This value includes the whole process chain of robot repeatability (for the initial point definition), precision of defining points by pivoting (for the subsequent OTS-based point definition), and the tool calibration precision (for tool tip-to-marker registration).

B. *Force-Based Deformation Estimation*

In the following, details of the stiffness estimation step (Subsection B.I) and their consequences for deformation estimation (Subsection B.II) are described.

B.I *Stiffness Estimation*

The stiffness of base, robot, tool holder, and miller along the three tool axes was determined by deforming the structure against a known ground truth, i.e. a fixed and rigid obstacle, and measuring the resulting forces. The range of interest for the absolute applied forces is about $|\boldsymbol{F}|$=0...35N for milling applications as a result of force-based speed control, aimed at limiting bone heat trauma [6], [8].

As the following results show that the observed force-to-deflection ratio is constant for the system setup and for the range of forces applied (Figure 6), there is no need to apply higher-order approximation functions or implement a lookup table for the deformations. A simple error estimator of the form

$$\Delta p_i(F_i) = \frac{1}{k_i} \cdot F_i, i = x, y, z$$

is sufficient (Table 1 lists the measured stiffness factors). The remaining position error (after deformation estimation) is below 0.25mm for all axes, while the worst non-corrected position measurement was over 1.75mm off for the force range under scrutiny, as seen from Figure 6.

Table 1: Measured structural stiffness along tool frame axes

Stiffness	k_x	k_y	k_z
	$17.52\frac{N}{mm}$	$19.27\frac{N}{mm}$	$86.66\frac{N}{mm}$

B.II *Deformation Estimation*

The measured stiffness is used to estimate the deformation error for the tool tip. A milling procedure has been executed for an actual implant-based excavation volume (Figure 3; generic path for Vibrant Soundbridge, Siemens/Symphonix, planned according to [20]) in samples of oak wood, which in former experiments has been shown to exhibit similar properties to human skull bone, except for hardness. The used miller head was a 4.5mm diameter spherical drill.

The occurring forces are highest along the *Z* axis, i.e. the miller's rotatory axis. The vertically-held miller has only little removal capability at its apex, which is desirable in everyday use because of the limited damage to the dura mater that can be inflicted this way. However, this also implies high reactive forces up and out of the milling excavation volume.

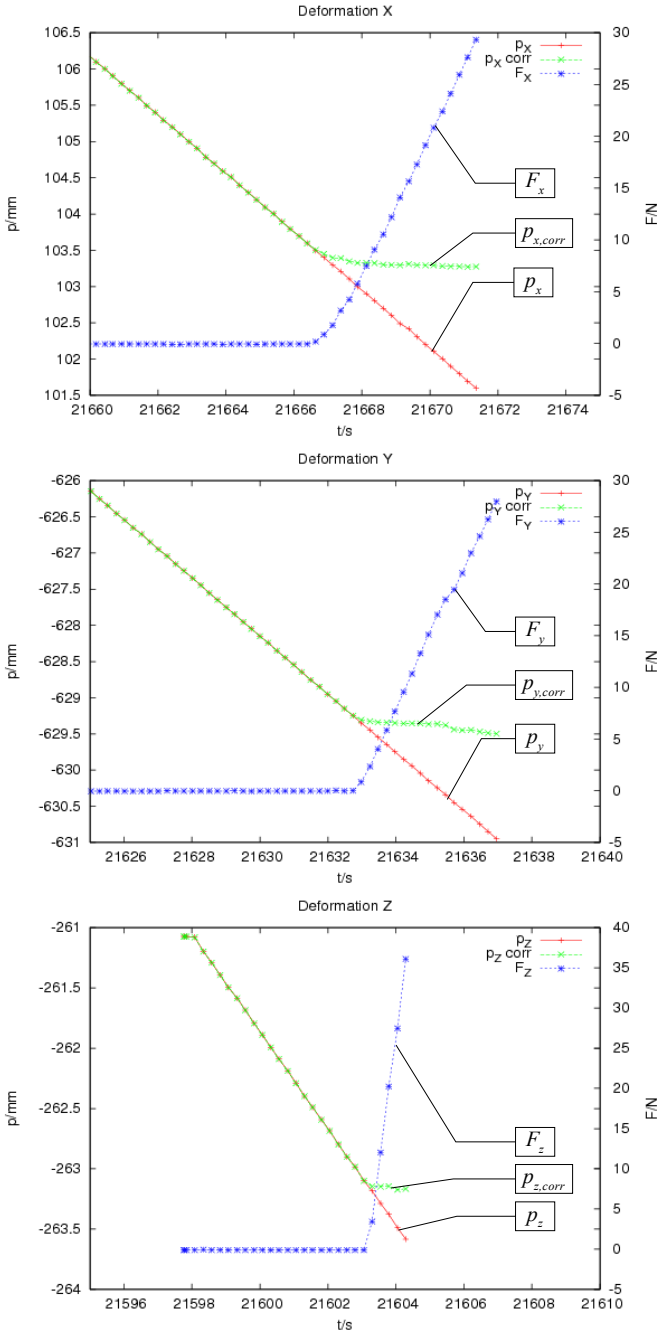

Figure 6: Expected position of the tool tip (red, „p_i“), applied forces (blue, „F_i“), and estimated position (green, „$p_{i,corr}$“) along tool axes X (top), Y (centre), and Z (bottom)

The effects can be seen in Figure 7, showing an enlarged side view of the recorded milling path, which consists of four distinct sinking iterations [20]. The effective position – including estimated deformation – consistently lies above the planned position during planar (*X*/*Y*) milling. The vertical (*Z*) feed motions show almost no lateral deformation. The effect becomes more pronounced with increasing milling depth (negative *Z*), where the miller head operates at higher removal rates. The maximum deformation observed during this experiment was ~0.45mm.

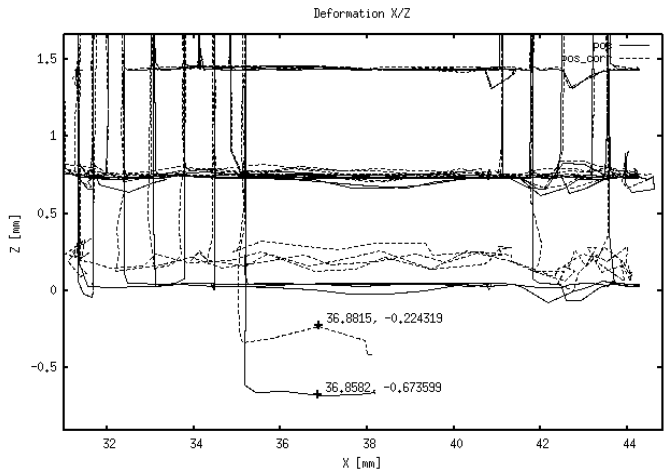

Figure 7: Enlarged side view (X/Z) of recorded milling motion (Soundbridge implant, four sinking iterations top-to-bottom); showing the difference between planned milling path (solid line) and effective path due to deformation (dotted line)

VII. Conclusions

The errors related to registration by optical tracking and deformation during robotic milling operations have been investigated and quantified. It has been shown that with the selected algorithms for OTS-based calibration and point definition (by sphere fitting), the achievable precision can be as high as 0.33mm for single markers (on top of the 0.05mm OTS repeatability accuracy), marking a lower limit for precision of OTS-based registration. When the robot is introduced into the loop, the errors grow, but remain small enough for the OTS to serve as dynamic registration insurance. For only three-point registration, the registration error of about 2...4mm may be sufficient when interventions are supported by intraoperative sensors. For 3D deformation, estimation functions have been determined, and experiments show their relevance for high-precision milling, as deformations in real use become at least as large as 0.45mm.

Future work includes the use of optically tracked pointers to define points for robot-OTS registration, surfaces, and trajectories for intraoperative procedures like ultrasound imaging. Instead of e.g. force-based servoing of the robot-held ultrasound probe along the surface to be scanned (similar to dermatome servoing in [4]), the imaging run can be accelerated by predefining the scan trajectory manually with pointers. Furthermore, dynamic registration (*tracking*) between camera, robot base, and the patient will be integrated to reduce the effects of sudden shifts of tracked objects or the OTS by controlling the robot position appropriately. This will also allow comparative measurements of deformation based on both force and OTS.

Acknowledgements

This work is a result of the project „Robot-based navigation for milling at the lateral skull base (RONAF)“ of the special research cluster „Medical navigation and robotics“ (SPP 1124) funded by the Deutsche Forschungsgemeinschaft (DFG), performed in cooperation with the Universitäts-HNO-Klinik (Abt. HNO-Heilkunde) in Heidelberg/Germany. Further information can be found at *http://ai3.inf.uni-bayreuth.de/projects/ronaf/*.

References

[1] M. De la Fuente, M. Hahndorff, T. Dahmen, S. Weltgen, D.C. Wirtz, F. Portheine, K. Radermacher, „Freehand Navigation using longshaft tools – comparing a force sensor based deflection compensation with an intramedular support device“, *CAOS International*, 2004.

[2] K. Denis, A. Ranftl, G. v. Ham, et al, „Comparison of Registration Procedures of the Tibia in Robot-Assisted Total Knee Arthroplasty“, *MICCAI 2003*, Montréal,QC/Canada, November 2003.

[3] P. Drouet, S. Dubowsky, C. Mavroidis, „Compensation of Geometric and Elastic Deflection Errors in Large Manipulators based on Experimental Measurements: Application to a High Accuracy Medical Manipulator“, *Robotica, vol 20, No. 3*, 2002.

[4] G. Duchemin, E. Dombre, F. Pierrot, Ph. Poignet, “Robotized Skin Harvesting”, *ISER 2002*, Sant'Angelo d'Ischia/Italy, 2002.

[5] D. Engel, J. Raczkowsky, H. Woern, „Sensor-aided Milling with a Surgical Robot System“, *CARS 2002*, Paris/France, June 2002.

[6] P.A. Federspil, C. De Mola, U.W. Geisthoff, D. Henrich, P.K. Plinkert, Ph. Stolka, „Force Feedback Control of Robot's Speed Prevents Heat Trauma in Robotic Milling at the Lateral Skull Base“, *CURAC 2003*, Nürnberg/Germany, 2003.

[7] P.A. Federspil, S.H. Tretbar, P.K. Plinkert, “Increase the Accuracy in Navigated Surgery by in site Measurement of individual Sound Velocity in Skull Bone”, *CURAC 2005*, Berlin/Germany, September 2005.

[8] A. Fuchsberger, “Untersuchung der spanenden Bearbeitung von Knochen”, *iwb Forschungsberichte Band 2*, Techn. Univ. München/Institut für Werkzeugmaschinen und Betriebswissenschaften, 1986.

[9] D. Henrich, “Robotergestütztes Fräsen an der lateralen Schädelbasis: Kraft-basierte lokale Navigation bei der Implantatbettanlage”, *Robotik 2002*, Ludwigsburg/Germany, June 2002.

[10] D. Henrich, Ph. Stolka, “Principles of Navigation in Surgical Robotics”, *MRVN 2004*, Remagen/Germany, March 2004.

[11] J. T. Lea et al., “Registration and immobilization in robot-assisted surgery”, *Journal of Image-Guided Surgery*, 1995.

[12] New River Kinematics, “COBRA Robot Deflection Modeling”, http://www.kinematics.com/custom_projects_cobra.htm

[13] J. E. Speich, J. Rosen, “Medical Robotics”, *Encyclopedia of Biomaterials and Biomedical Engineering*, 2004.

[14] Ph. Stolka, D. Henrich, “A Hybrid Force-Following Scheme for Multi-Scale Motions”, *SYROCO 2003*, Wrocław/Poland, September 2003.

[15] Ph. Stolka, D. Henrich, “Building Local Maps in Surgical Robotics”, *IROS 2005*, Edmonton,AB/Canada, August 2005.

[16] R.H. Taylor et al, „An image-directed robotic system for precise orthopaedic surgery“, *IEEE Transactions on Robotics and Automation 10(3):261-275*, June 1994.

[17] R. H. Taylor, D. Stoianovici, “Medical Robotics in Computer-Integrated Surgery”, *IEEE Transactions on Robotics and Automation*, Vol. 19, No. 5, Oct. 2003.

[18] D. Umbach, K.N. Jones, “A Few Methods for Fitting Circles to Data”, *IEEE Transactions on Instrumentation and Measurement*, 2000.

[19] M. Waringo, Ph. Stolka, D. Henrich, “First System for Interactive Position Planning of Implant Components“, *CURAC 2003*, Nürnberg/Germany, 2003.

[20] M. Waringo, D. Henrich, „3-Dimensionale schichtweise Bahnplanung für Anytime-Fräsanwendungen“, *CURAC 2003*, Nürnberg/Germany, 2003.